COMPDYN 2015
5th ECCOMAS Thematic Conference on
Computational Methods in Structural Dynamics and Earthquake Engineering
M. Papadrakakis, V. Papadopoulos, V. Plevris (eds.)
Crete Island, Greece, 25–27 May 2015

PLANE WAVE AT THE INTERFACE BETWEEN WATER AND A GASSY POROELASTIC LAYER WITH UNDERLYING ELASTIC SEABED

Weiyun Chen[1], **Guoxing Chen**[1]

[1] Institute of Geotechnical Engineering, Nanjing Tech University, Nanjing 210009, China;

e-mail: vic_chen@126.com

Keywords: Plane wave, Reflection coefficient, Gassy marine sediments, Ocean floor;

Abstract. *Based on the multiphase poroelasticity theory, the reflection characteristics of an obliquely incident plane wave upon a plane interface between overlying water and a gassy marine sediment layer with underlying elastic solid seabed are investigated. The sandwiched gassy layer is modeled as a porous material with finite thickness, which is saturated by two compressible and viscous fluids (liquid and gas). The closed-form expression for the amplitude ratio of the reflected wave, i.e., reflection coefficient, is derived according to the boundary conditions at the upper and lower interfaces in the proposed model. Using numerical calculation, the influences of incident angle, wave frequency, layer thickness and liquid saturation of sandwiched porous layer on the reflection coefficient are analyzed, respectively. It is revealed that the reflection coefficient is closely associated with incident angle and sandwiched layer thickness. Moreover, in different frequency ranges, the dependence of the wave reflection characteristics on moisture (or gas) variations in the intermediate marine sediment layer is distinguishing.*

1 INTRODUCTION

Wave reflection coefficient is an important parameter representing the quantitative characterization of the geoacoustic properties of the seabed sediment and its subbottom structure. During the past several decades, the subject of plane reflection from the ocean floor is important in the applications such as geophysics, seismology, underwater acoustics, petroleum engineering, and hydrogeology [1-6]. The fundamental theory of the elastic plane wave propagation in fluid-saturated porous media was initially introduced by Biot who predicted the existence of three types of bulk waves propagating in the fluid-filled porous material: P1 wave, P2 wave and S wave [7]. The P2 wave was observed firstly in sintered glass beads [8] and then in natural air-filled sand-stone [9]. Based on Biot theory and its extension to unsaturated media, the transmission and reflection of bulk waves at the boundary between water and fluid-saturated porous sediment were discussed [2,10,11,12] Stoll & Kan investigated the reflection and transmission of seismic waves at interface between water and a material which is believed to be a realistic model of marine sediment [2]. Albert compared two different interfaces, the air/air-filled porous medium and the water/water-saturated porous medium [13]. Denneman et al. studied the wave properties at a fluid/porous-medium interface through simple closed-form expressions for the reflection and transmission coefficients [14]. From the Biot - Gassmann theory for fluid-saturated porous rocks, Russell et al. first derived a general formula for fluid-property discrimination and combined it with an AVO inversion to show its geophysical applications in the extraction of information about the fluid properties of the reservoir. Considering volume scattering, Ohkawa et al. studied the reflection and transmission coefficients at the surface of sandy seabed [16] and then Ohkawa [12] confirmed the efficiency of Biot theory to describe wave problems in water-saturated granular marine sediment. Dai & Kuang obtained the reflection and transmission coefficients at the interface between water and double porosity solid half-space [17].

In these aforementioned studies, the seabed model was regarded as a isotropic and homogeneous porous half-space. More often, though, ocean floor is covered by the marine sediment layer with finite thickness, which can be considered as multi-phase porous medium consisting of solid skeleton and two compressible and viscous fluids (i.e., liquid and gas). Thus some other researches were also carried out by modeling the ocean floor as layered sediments with an underlying substrate. Kuo used an plane wave scattering model for three homogeneous layers consisting of a thin solid sediment layer sandwiched by semi-infinite water and solid basalt media [18]. Ainslie derived the simple expressions of wave reflection and transmission coefficients for a layered fluid sediment layer sandwiched between a uniform fluid above and a uniform solid substrate below[19]. Wang et al. [20] and Lyu et al. [21] investigated plane wave propagation at the interface between water and porous sediment with an underlying solid substrate and double porosity substrate, respectively.

However, it has been extensively accepted that some natural sedimentary materials are not fully saturated by liquid. The above-mentioned literatures modeling the ocean floor as layered seabed sediments with an underlying half-space seldom took the moisture (or gas) variations of marine sediment layer into account. The model of Boyle & Chotiros [22] found that very small amounts of gas were sufficient to dominate other wave scattering mechanisms from the ocean floor. In fact, Biot theory did not involve the case when two different immiscible phase fluids coexist in the interstice of porous sedment. Due to the appearance of gas phase, besides two longitudinal waves (P1 wave and P2 wave) and one transverse wave (S wave) in Biot theory, which appear in the fully liquid-saturated porous medium, an additional longitudinal wave (P3 wave) emerges [23-27]. Based on the three-phase porous theory, reflection and

transmission phenomenon of incident waves at the plane surface of semi-infinite porous material were discussed [28,29].

Until now, to the best of our knowledge, no investigation have been launched to study the reflection and transmission of plane waves at the plane interface between water and ocean floor comprising an upper gassy poroelastic layer and underlying elastic seabed. The purpose of the present paper is to discuss this issue. This problem is meaningful and essential for exploring oil, gas, or water contained in the fissured rocks of the ocean floor. Our procedure is formulated within the framework of the continuum theory of mixtures. The closed-form expressions for the amplitude ratios of reflected and transmitted plane waves are derived based on the linear viscoporoelastic model [27, 29]. In a systematic manner, these coefficients are then used to analyze the influences of incident angle, wave frequency, layer thickness and liquid saturation of sandwiched porous layer on the wave reflection characteristics upon the gassy poroelastic layer, respectively.

2 BASIC WAVE THEORY

The following analytical process is carried out basing on the standard elastic wave analysis. Fig. 1 shows the coordinate system for the problem of plane wave incidence, reflection and transmission. This system comprises the overlying water, the poroeastic sediment layer containing free gas, and the underlying solid seabed. The overlying water is assumed as ideal compressible fluid. The sandwiched sediment layer is modeled as linear three-phase porous medium with finite thickness H. The underlying substrate is considered as linear elastic solid half-space. Here, z axis is directed vertically upwards and the x axis is assumed along horizontal direction as shown in Fig. 1. $z = 0$ and $z = -H$ represent two plane interfaces separating the overlying water, the gassy poroelastic layer and the underlying solid half-space, respectively. The interface along $z = -H$ is in perfect contact in such a way that the fluid cannot flow from porous medium to the solid substrates.

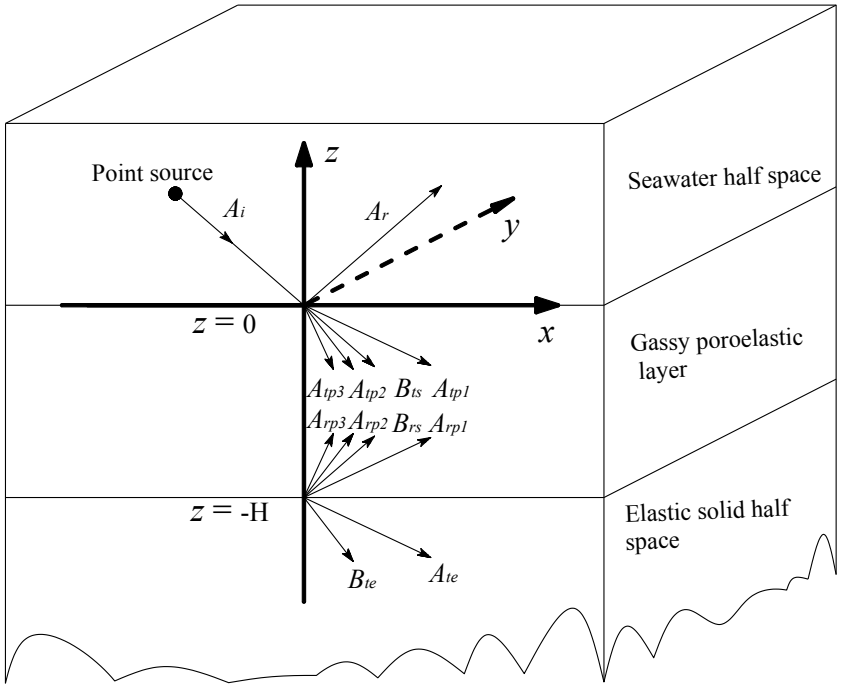

Figure 1. Coordinate system for the incident, reflected and transmitted waves

2.1. Sandwiched gassy poroelastic layer

In this paper, the sandwiched gassy poroelastic medium is considered as a mixture consisting of a deformable solid frame, a liquid phase and a gas phase, designated by the superscripts "*S*", "*L*", and "*G*", respectively. The character α is used to denote an individual phase, i.e., α = *S*, *L*, *G*. In the framework of the multiphase continuum theory [23, 25, 30], the motion equations for the gassy poroelastic medium, which can degenerate to the form of Biot model in fully liquid-saturated state, are given [27,29]:

$$\begin{pmatrix} n_S\rho_S & 0 & 0 \\ 0 & n_L\rho_L & 0 \\ 0 & 0 & n_G\rho_G \end{pmatrix}\begin{pmatrix} \ddot{\mathbf{u}}^S \\ \ddot{\mathbf{u}}^L \\ \ddot{\mathbf{u}}^G \end{pmatrix}+\begin{pmatrix} \xi_L+\xi_G & -\xi_L & -\xi_G \\ -\xi_L & \xi_L & 0 \\ -\xi_G & 0 & \xi_G \end{pmatrix}\begin{pmatrix} \dot{\mathbf{u}}^S \\ \dot{\mathbf{u}}^L \\ \dot{\mathbf{u}}^G \end{pmatrix}$$

$$=\begin{pmatrix} (r_{SS}+n_S\lambda_S+n_S\mu_S)\nabla(\nabla\cdot\mathbf{u}^S)+n_S\mu_S\nabla^2\mathbf{u}^S+r_{SL}\nabla(\nabla\cdot\mathbf{u}^L)+r_{SG}\nabla(\nabla\cdot\mathbf{u}^G) \\ r_{SL}\nabla(\nabla\cdot\mathbf{u}^S)+r_{LL}\nabla(\nabla\cdot\mathbf{u}^L)+r_{LG}\nabla(\nabla\cdot\mathbf{u}^G) \\ r_{SG}\nabla(\nabla\cdot\mathbf{u}^S)+r_{LG}\nabla(\nabla\cdot\mathbf{u}^L)+r_{GG}\nabla(\nabla\cdot\mathbf{u}^G) \end{pmatrix}, \tag{1}$$

where ∇ and ∇^2 are the gradient operator and Laplace operator in the Cartesian coordinate, respectively. $\mathbf{u}^\alpha$ (α = *S*, *L*, *G*) represents the displacement vector of α phase; $\dot{}$ and $\ddot{}$ denote the velocities and accelerations of individual component, respectively. ρ_α is the material density of α phase; λ_S and μ_S are the classical Lamé's constants of the empty porous solid; n_α denotes the fraction of the volume occupied by α phase; ξ_L and ξ_G are the drag force parameters representing the viscous dissipation between the fluids (liquid and gas) and the solid skeleton, respectively, the detailed expressions of which can be found in the references [25, 31, 32]. r_{SS}, r_{LL}, r_{GG}, r_{SL}, r_{SG} and r_{LG} are the coefficients pertinent to the coupling between different phases and can be determined from the relationships between them and the measurable parameters, which was detailed discussed in the porosity theory [27].

With the aid of the usual Helmholtz resolution of a vector, the three displacement vectors can be conveniently written in the following forms:

$$\mathbf{u}^\alpha=\nabla\psi_\alpha+\nabla\times\mathbf{H}_\alpha,\quad \nabla\cdot\mathbf{H}_\alpha=0, \tag{2}$$

where ψ_α and $\mathbf{H}_\alpha$ (α = *S*, *L*, *G*) are the scalar and vector potential functions for the solid, liquid and gas phases, respectively.

Substituting Eq. (2) into Eq. (1) and then applying divergence and curl operators to both sides of Eq. (1) respectively, we obtain

$$\begin{pmatrix} n_S\rho_S & 0 & 0 \\ 0 & n_L\rho_L & 0 \\ 0 & 0 & n_G\rho_G \end{pmatrix}\begin{pmatrix} \ddot{\psi}_S \\ \ddot{\psi}_L \\ \ddot{\psi}_G \end{pmatrix}+\begin{pmatrix} \xi_L+\xi_G & -\xi_L & -\xi_G \\ -\xi_L & \xi_L & 0 \\ -\xi_G & 0 & \xi_G \end{pmatrix}\begin{pmatrix} \dot{\psi}_S \\ \dot{\psi}_L \\ \dot{\psi}_G \end{pmatrix}=\nabla^2\begin{pmatrix} r_{SS}+n_S\lambda_S+2n_S\mu_S & r_{SL} & r_{SG} \\ r_{SL} & r_{LL} & r_{LG} \\ r_{SG} & r_{LG} & r_{GG} \end{pmatrix}\times\begin{pmatrix} \psi_S \\ \psi_L \\ \psi_G \end{pmatrix} \tag{3}$$

and

$$\begin{pmatrix} n_S\rho_S & 0 & 0 \\ 0 & n_L\rho_L & 0 \\ 0 & 0 & n_G\rho_G \end{pmatrix}\begin{pmatrix} \ddot{\mathbf{H}}_S \\ \ddot{\mathbf{H}}_L \\ \ddot{\mathbf{H}}_G \end{pmatrix}+\begin{pmatrix} \xi_L+\xi_G & -\xi_L & -\xi_G \\ -\xi_L & \xi_L & 0 \\ -\xi_G & 0 & \xi_G \end{pmatrix}\begin{pmatrix} \dot{\mathbf{H}}_S \\ \dot{\mathbf{H}}_L \\ \dot{\mathbf{H}}_G \end{pmatrix}=\nabla^2\begin{pmatrix} n_S\lambda_S & 0 & 0 \\ 0 & 0 & 0 \\ 0 & 0 & 0 \end{pmatrix}\begin{pmatrix} \mathbf{H}_S \\ \mathbf{H}_L \\ \mathbf{H}_G \end{pmatrix}. \tag{4}$$

Eqs. (3) and (4) describe the propagation of the P wave and S wave in three-phase porosity media, respectively. The general solutions of Eqs. (3) and (4) are of the forms:

$$\psi_\alpha=A_\alpha\exp[\mathrm{i}k_p(lx+nz-c_pt)], \tag{5}$$

$$\mathbf{H}_{\alpha} = \mathbf{B}_{\alpha} \exp[\mathrm{i}k_s(lx + nz - c_s t)], \tag{6}$$

where $\mathrm{i} = \sqrt{-1}$; k_p and k_s are the wave numbers of P wave and S wave respectively; l and n are the values of direction vectors; c_p and c_s are the phase velocities of the P wave and S wave respectively.

Substituting Eq. (5) into Eq. (3), we get the following characteristic equation for P wave:

$$\det[A] = 0, \tag{7}$$

where $[A]$ is a symmetric matrix of order 3×3 with its elements given by

$$a_{11} = \mathrm{i}\omega(\xi_L + \xi_G) + \omega^2\rho_S - k_p{}^2(r_{SS} + n_S\lambda_S + 2n_S\mu_S),\ a_{22} = \mathrm{i}\omega\xi_L + \omega^2\rho_L - k_p{}^2 r_{LL},$$

$$a_{33} = \mathrm{i}\omega\xi_G + \omega^2\rho_G - k_p{}^2 r_{GG},\ a_{12} = a_{21} = -\mathrm{i}\omega\xi_L - k_p{}^2 r_{SL},$$

$$a_{13} = a_{31} = -\mathrm{i}\omega\xi_G - k_p{}^2 r_{SG},\ a_{23} = a_{32} = -k_p{}^2 r_{LG}.$$

In a similar manner, substituting Eq. (6) into Eq. (4), the following characteristic equation for S wave is derived:

$$\det[B] = 0, \tag{8}$$

where $[B]$ is also a symmetric matrix of order 3×3, its entries are given by

$$b_{11} = \mathrm{i}\omega(\xi_L + \xi_G) + \omega^2\rho_S - n_S\mu_S k_s{}^2,\ b_{22} = \mathrm{i}\omega\xi_L + \omega^2\rho_L,\ b_{33} = \mathrm{i}\omega\xi_G + \omega^2\rho_G,$$

$$b_{12} = b_{21} = -\mathrm{i}\omega\xi_L,\ b_{13} = b_{31} = -\mathrm{i}\omega\xi_G,\ b_{23} = b_{32} = 0.$$

Eqs. (7) and (8) indicate in a physical sense that there exist one type of S wave and three types of P wave in the sandiwiched elastic porous layer containing two immiscible fluids, typically denoted as P1 wave, P2 wave and P3 wave in descending order of phase speed [23, 25,26,27].

In an isotropic three-phase porous medium, the constitutive expressions representing the stress-strain relationships take the following forms [27]:

$$\boldsymbol{\sigma}^S = [(r_{SS} + n_S\lambda_S)\nabla^2\psi_S + r_{SL}\nabla^2\psi_L + r_{SG}\nabla^2\psi_G]I + 2n_S\mu_S\varepsilon_S, \tag{9}$$

$$-p^L = (r_{SL}\nabla^2\psi_S + r_{LL}\nabla^2\psi_L + r_{LG}\nabla^2\psi_G)I, \tag{10}$$

$$-p^G = (r_{SG}\nabla^2\psi_S + r_{LG}\nabla^2\psi_L + r_{GG}\nabla^2\psi_G)I, \tag{11}$$

where $\boldsymbol{\sigma}^S$ is the stress in porous solid; p^L and p^G are the pressures of liquid and gas respectively; I is unit tensor matrix. ε_S denotes the strain tensor of the solid skeleton, i.e., $\varepsilon_S = \frac{1}{2}[\nabla\mathbf{u}^S + (\nabla\mathbf{u}^S)^T]$, the superscript T represents the transpose.

2.2. Overlying seawater half-space

The motion equation of overlying water has the following form:

$$\rho_W \ddot{\quad} \quad \nabla\nabla\cdot\mathbf{u}^W, \tag{12}$$

where K_W is the bulk modulus of the water, ρ_W is the water density and $\mathbf{u}^W$ is its displacement vector.

The fluid pressure in the upper water is

$$p_W = -K_W\nabla\cdot\mathbf{u}^W. \tag{13}$$

2.3. Underlying elastic half-space

The underlying elastic half-space represents the bedrock under the shallow poroelastic sediment layer and has the governing equation as:

$$(\lambda_E + \mu_E)\nabla\nabla\cdot\mathbf{u}^E + \mu_E\nabla^2\mathbf{u}^E = \rho_E\ddot{} \quad , \tag{14}$$

where λ_E and μ_E are Lame's constants, ρ_E is the solid density, and $\mathbf{u}^E$ is the displacement vector with the following form:

$$\mathbf{u}^E = \nabla\psi_E + \nabla\times\mathbf{H}_E\,, \tag{15}$$

where ψ_E and $\mathbf{H}_E$ are the scalar and vector displacement potentials, respectively.

3 BOUNDARY CONDIIONS

As depicted in Fig. 1, a plane P wave (plane wave) propagates through the upper water half-space and then impinges upon the interface (z = 0) with an angular frequency ω and an angle of incidence θ_i. In this circumstance, one reflected P wave (plane wave) is generated in the overlying water (z > 0). Furthermore, according to Eqs. (7) and (8), four transmitted bulk waves from the upper interface and four reflected bulk waves from the lower interface are predicted to be excited in the sandwiched gassy poroelastic layer (-H < z < 0) and two transmitted waves exist in the elastic substrate (z < -H). Accordingly, the displacement potential functions of the incident, reflected and transmitted waves can be expressed as:
(i) In the overlying water (z > 0):

$$\psi_W = A_i\exp[\mathrm{i}k_{ip}(l_{ip}x - n_{ip}z - c_{ip}t)] + A_r\exp[\mathrm{i}k_{rp}(l_{rp}x + n_{rp}z - c_{rp}t)]\,, \tag{16a}$$

(ii) In the gassy poroelastic layer (-H < z < 0):

$$\psi_S = \sum_{n=1}^{3}A_{tpn}^S\exp[\mathrm{i}k_{tpn}(l_{tpn}x - n_{tpn}z - c_{tpn}t)] + \sum_{n=1}^{3}A_{rpn}^S\exp[\mathrm{i}k_{rpn}(l_{rpn}x + n_{rpn}z - c_{rpn}t)]\,, \tag{16b}$$

$$\psi_L = \sum_{n=1}^{3}A_{tpn}^L\exp[\mathrm{i}k_{tpn}(l_{tpn}x - n_{tpn}z - c_{tpn}t)] + \sum_{n=1}^{3}A_{rpn}^L\exp[\mathrm{i}k_{rpn}(l_{rpn}x + n_{rpn}z - c_{rpn}t)]\,, \tag{16c}$$

$$\psi_G = \sum_{n=1}^{3}A_{tpn}^G\exp[\mathrm{i}k_{tpn}(l_{tpn}x - n_{tpn}z - c_{tpn}t)] + \sum_{n=1}^{3}A_{rpn}^G\exp[\mathrm{i}k_{rpn}(l_{rpn}x + n_{rpn}z - c_{rpn}t)]\,, \tag{16d}$$

$$H_S = B_{ts}^S\exp[\mathrm{i}k_{ts}(l_{ts}x - n_{ts}z - c_{ts}t)] + B_{rs}^S\exp[\mathrm{i}k_{rs}(l_{rs}x + n_{rs}z - c_{rs}t)]\,, \tag{16e}$$

$$H_L = B_{ts}^L\exp[\mathrm{i}k_{ts}(l_{ts}x - n_{ts}z - c_{ts}t)] + B_{rs}^L\exp[\mathrm{i}k_{rs}(l_{rs}x + n_{rs}z - c_{rs}t)]\,, \tag{16f}$$

$$H_G = B_{ts}^G\exp[\mathrm{i}k_{ts}(l_{ts}x - n_{ts}z - c_{ts}t)] + B_{rs}^G\exp[\mathrm{i}k_{rs}(l_{rs}x + n_{rs}z - c_{rs}t)]\,, \tag{16g}$$

(iii) In the elastic substrate (z < -H)

$$\psi_E = A_{pe}\exp[\mathrm{i}k_{pe}(l_{pe}x - n_{pe}z - c_{pe}t)]\,, \tag{16h}$$

$$H_E = B_{se}\exp[\mathrm{i}k_{se}(l_{se}x - n_{se}z - c_{se}t)]\,. \tag{16i}$$

where the subscripts i, r and t refer to the quantities corresponding to the incidence, reflection and transmission, respectively.

Substituting Eqs. (16b) – (16g) into Eqs. (7) and (8), we obtain the following relations between the various values of the amplitudes of reflected and transmitted waves:

$$\delta_{Ln} = \frac{A^L_{rpn}}{A^S_{rpn}} = \frac{A^L_{tpn}}{A^S_{tpn}} = \frac{a^{(n)}_{13}a^{(n)}_{22} - a^{(n)}_{23}a^{(n)}_{12}}{a^{(n)}_{23}a^{(n)}_{11} - a^{(n)}_{13}a^{(n)}_{21}},\ (n = 1, 2, 3) \tag{17a}$$

$$\delta_{Gn} = \frac{A^G_{rpn}}{A^S_{rpn}} = \frac{A^G_{tpn}}{A^S_{tpn}} = \frac{a^{(n)}_{32}a^{(n)}_{21} - a^{(n)}_{22}a^{(n)}_{31}}{a^{(n)}_{22}a^{(n)}_{33} - a^{(n)}_{23}a^{(n)}_{32}},\ (n = 1, 2, 3) \tag{17b}$$

$$\delta_{LS} = \frac{B^L_{rs}}{B^S_{rs}} = \frac{B^L_{ts}}{B^S_{ts}} = -\frac{b_{22}}{b_{21}}, \tag{17c}$$

$$\delta_{GS} = \frac{B^G_{rs}}{B^S_{rs}} = \frac{B^G_{ts}}{B^S_{ts}} = \frac{b_{21}b_{12} - b_{11}b_{22}}{b_{13}b_{22}}. \tag{17d}$$

When Eqs. (17a) – (17d) are combined with Eqs. (16a) – (16i), there remain unknown complex amplitudes which could be determined by considering the boundary conditions. These boundary conditions concerning stress and displacement components need to insure the continuity across the upper and lower plane interfaces at $z = 0$ and $z = -H$. Due to the difficulty to determine the fluid flow impedance across the interface between overlying water and gassy poroelastic layer [3], sealed-pore boundary condition is employed here for simplicity.

The interface between the overlying water and gassy poroelastic layer ($z = 0$) yields

continuity of normal stress: $\boldsymbol{\sigma}^S_{zz} = -p_W$; (18a)

continuity of normal displacement: $\mathbf{u}^S_z = \mathbf{u}^W_z$; (18b)

disappearance of relative displacements: $\mathbf{u}^L_z - \mathbf{u}^S_z = 0$, $\mathbf{u}^G_z - \mathbf{u}^S_z = 0$; (18c,d)

disappearance of tangential stress: $\boldsymbol{\sigma}^S_{xz} = 0$; (18e)

The interface between the gassy poroelastic layer and underlying solid half-space (z = -H) yields

continuity of normal displacement: $\mathbf{u}^S_z = \mathbf{u}^E_z$; (18f)

continuity of tangential displacement: $\mathbf{u}^S_x = \mathbf{u}^E_x$; (18g)

continuity of tangential stress: $\boldsymbol{\sigma}^S_{xz} = \boldsymbol{\sigma}^E_{xz}$; (18h)

continuity of normal stress: $\boldsymbol{\sigma}^S_{zz} = \boldsymbol{\sigma}^E_{zz}$; (18i)

disappearance of relative displacements: $\mathbf{u}^L_z - \mathbf{u}^S_z = 0$, $\mathbf{u}^G_z - \mathbf{u}^S_z = 0$; (18j,k)

Combining the potential functions (16a) – (16i) and the boundary conditions (18a) – (18k) and then considering Snell's law at the interface, we get the following set of equations:

$$[M][A_r, A^S_{tp1}, A^S_{tp2}, A^S_{tp3}, A^S_{rp1}, A^S_{rp2}, A^S_{rp3}, B^S_{ts}, B^S_{rs}, A_{te}, B_{te}]^T = A_i[Q], \tag{19}$$

where the corresponding elements in the matrixes $[M]$ and $[Q]$ are given in Appendix.

4 NUMERICAL RESULTS AND DISCUSSION

In order to investigate the dependence of the amplitude coefficient of the reflected waves (i.e., A_r / A_i) on the incident angle, frequency, liquid saturation of the porous layer, and the layer thickness, a numerical study is carried out by Matlab. In fact, the energy of the incident and reflected wave in the seawater is proportional to the amplitude. So the amplitude reflec-

tion coefficient in this paper could also express the fraction of the energy of the reflected wave. And this methodology has the potential to be used on real data through AVO analysis. Based on the method of Fatti et al [33], Russell, et al. [34] estimated the P and S-wave impedances using a standard inversion technique. The material parameters needed in the numerical simulation are summarized in Table. 1. The reflection coefficient is calculated with respect to the various model parameters from the formulas derived in the previous section.

It is worth noting that, when the excitation frequency ω exceeds a certain transition frequency ω_c, the viscous coupling coefficient becomes frequency-dependent and the frequency correction should be introduced. The transition frequency for the porous medium saturated by two immiscible fluids is defined as $\omega_c = \tau^{-1}$ [36], where τ is considered as the sum of two "damping time scales" for liquid and gas in the pore as:

$$\tau = \tau_L + \tau_G = k(\rho_L k_r^L / \eta_L + \rho_G k_r^G / \eta_G). \tag{20}$$

where k is the intrinsic permeability of the porous medium; η^F ($F = L,G$) is the fluid viscosity; k_r^F is the relative permeability simplified to be a function of saturation. So the transition frequency ω_c can be viewed as a function of water saturation. Based on the material parameters given in table 1, the transition frequency corresponding to the various water saturations (from 0 to 1) is calculated to be: $\omega_c \geq 3.3\times10^6$ rad/s. In the following calculations, the wave excitation frequency is restricted to be: $f \leq$ 1000Hz, which is much smaller than the minimum value of transition frequency ω_c. As discussed above, in this "low frequency range", the effect of the frequency correction factor can be negligible.

Table 1 Material properties of the model

Overlying water
$\rho_W = 1000\text{kg/m}^3$, $K_W = 2.2\text{GPa}$,
Elastic solid half-space
$\mu_E = 5\text{GPa}$, $\lambda_E = 12\text{GPa}$, $\rho_E = 2460\,\text{kg/m}^3$,
Sandwiched poroelastic medium
$n = 0.3$, $\rho_S = 2650\,\text{kg/m}^3$, $\rho_L = 1000\ \text{kg/m}^3$, $\rho_G = 1.2\,\text{kg/m}^3$, $K_S = 36\,\text{GPa}$,
$K_L = 2.2\,\text{GPa}$, $K_G = 0.1\,\text{MPa}$, $k = 3.0\times10^{-13}\ \text{m}^2$, $\eta^G = 1.8\times10^{-5}\ \text{Pa}\cdot\text{s}$, $\eta^L = 0.001\ \text{Pa}\cdot\text{s}$.
$\lambda_S = 9.0\,\text{GPa}$, $\mu_S = 4.0\,\text{GPa}$, $m_{vg} = 0.5$, $\alpha_{vg} = 0.0001\,\text{Pa}^{-1}$, $k = 3\times10^{-13}\,\text{m}^2$.

4.1 Bulk waves in the gassy poroelastic layer

From the characteristic equations (7) and (8), the propagation speed and attenuation of the four bulk waves, typically characterized as P1, P2, P3 and S waves, can be analyzed. In the limiting case for a complete saturation, the motion equation (1) can be reduced to a simpler form of classic Biot model, which was discussed by Chen et al. [22]. Among these four bulk waves, P1 wave travels fastest with lowest attenuation, which is similar to the fast P wave in the Biot theory. In the context of the Biot-Gassmann theory, Russell et al. [34] only considered the fast P wave when calculated P-wave velocity in the saturated porous medium. Similarly, since the P1 wave are analogous to the regular P wave in elastic solid, the other P2 and P3 waves are negligible when this methodological investigation is developed in geophysical applications. The phase velocities of P1 and S waves are several orders magnitude lager than those of P2 and P3 waves, while their attenuation coefficients are several orders magnitude smaller than those of P2 and P3 waves [27]. Thus, the P1 wave and S wave occupy the vast majority of the transmitted wave energy across the interface at $z = 0$. Base on the physical pa-

rameters listed in Table 1, Fig. 2 shows the frequency-dependent and saturation-dependent behavior of P1 and S waves in the gassy poroelastic layer. The attenuation coefficient is denoted by the imaginary part of the corresponding complex wave number. The liquid saturation considered here is from 20% to 99.99% and the frequency is taken to be 1 Hz, 10 Hz, 100 Hz and 1000Hz, respectively. As depicted in Figs. 2 (a), the speed of P1 wave is independent of frequency and decreases almost linearly during the change of saturation in the unsaturated case and then increases abruptly when it is close to the fully saturated case. The attenuation of P1 wave almost bears the opposite trend compared with its propagation speed. In Fig. 2 (b), the S wave speed decreases linearly with liquid saturation degree. The attenuation of both P1 and S waves increases with increasing frequency. Like P1 wave, the wave speed of S wave is frequency-independent and its attenuation increases with increasing saturation.

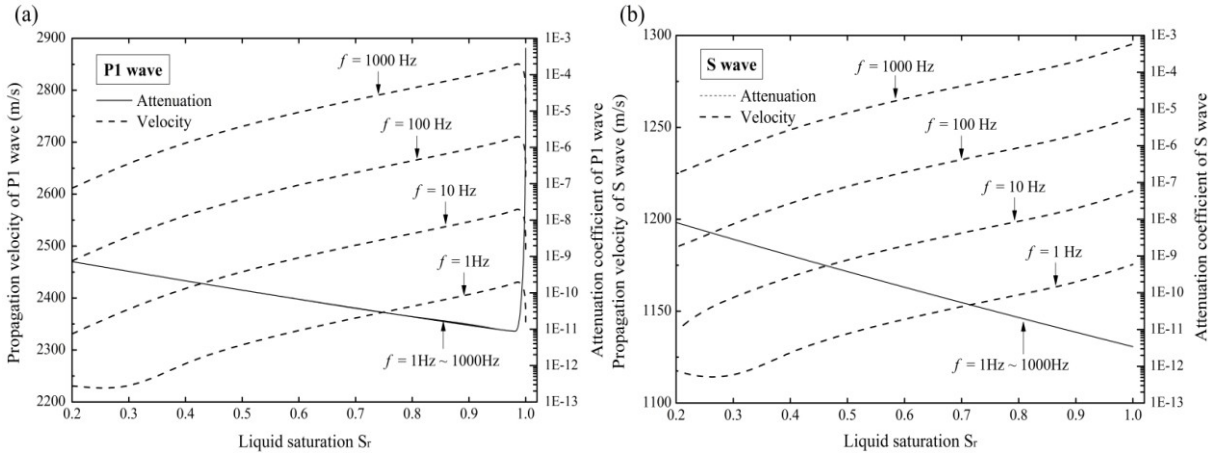

Figure 2. Variation of acoustic velocity (refer to left axes) and attenuation coefficient (refer to right axes) with liquid saturation of the gassy poroelastic layer for: (a) P1 wave, (b) S wave.

4.2 Variation of reflection coefficient with the incident angle

Fig. 3 shows the variation of the magnitude of the reflection coefficient A_r / A_i with incident angle θ_i using Eq. (19). The frequency f is set to be 100Hz and the liquid saturation of the porous layer Sr is 90%. Four different layer thicknesses: H = 0m, 5m, 50m and 500m are discussed, respectively. For the physical parameters listed in Table 1, the speed of the incident wave in the overlying water v_i is 1483.2 m/s, the speeds of P and S wave in the underlying elastic half-space are 2990.5 and 1425.7m/s, respectively. The speeds of P1 and S waves in the intermediate gassy porous layer are 2366.8 and 1147.9m/s, respectively. We note in passing that, for the traditional wave reflection and transmission problem at the interface between two semi-infinite half-spaces, the angles of incidence and emergence are related by Snell's law. When one of the angles corresponding to a reflected or transmitted wave increases to 90°, a critical angle of incidence is defined as θ_{cr} for the generating wave. The critical angle for the incident P wave (plane wave) discussed in our paper can be determined from: $\theta_{cr} = \sin^{-1}(v_i / v_t)$, where v_i and v_t are the speeds of the incident and transmitted waves, respectively. When the incident angle θ_i equals to critical angle θ_{cr}, the transmitted wave becomes evanescent and the normal to the wavefront becomes theoretically horizontal. In this paper, when the gassy porous sediment is absent (H = 0), the considered layered model reduces to the wave problem at the interface between upper water and underlying elastic solid half-space. In this case, one critical incident angle exists for the incident wave as θ_{cr1} = 29.7°. In the other limiting case,

when the thickness of porous layer H approaches infinity, our model corresponds to the wave reflection and transmission at the water/porous-medium interface. And the corresponding value of the critical incident angle θ_{cr2} =38.8°. As shown in Fig. 3, with regard to the thickness of the porous layer H equals to 0m, the reflection coefficient has a maximum value at $\theta_i = \theta_{cr1}$. When the gassy porous layer becomes more thick, such as H = 50m and 500m, it achieves a maximum value around $\theta_i = \theta_{cr2}$. It is probably because that, with the thickness of the interface layer increasing, the calculation results appear to be more close to the aforementioned model, i.e., water/gassy porous-medium interface model with a fixed critical angle θ_{cr2}.

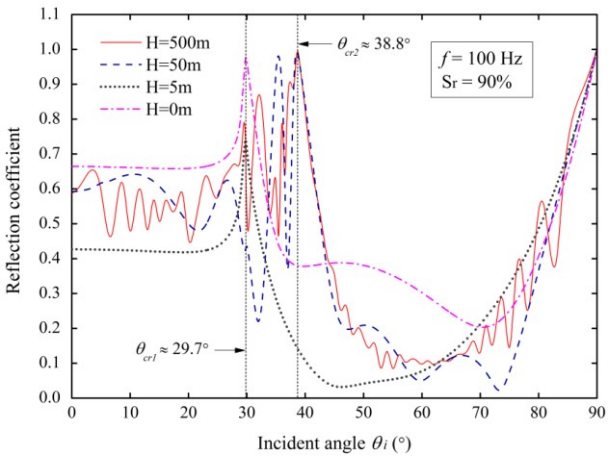

Figure 3. Reflection coefficient (A_r / A_i) as a function of incident angle θ_i for four different layer thicknesses: H = 0m, 5m, 50m and 500m.

Fig. 4 depicts the variation of reflection coefficient with the incident angle at three different liquid saturations of the gassy porous layer: Sr =80%, 90% and 99.99%. The thickness of the porous layer is set as 50m and the frequency f is 100Hz. When the interstices of the porous medium is almost filled with water, i.e., Sr =99.99%, the calculated result differs greatly from those of the other two cases. It is shown that, when the intermediate porous layer approaches totally liquid saturated, the reflection coefficient attains its maximal value near θ_{cr1} = 29.7°.

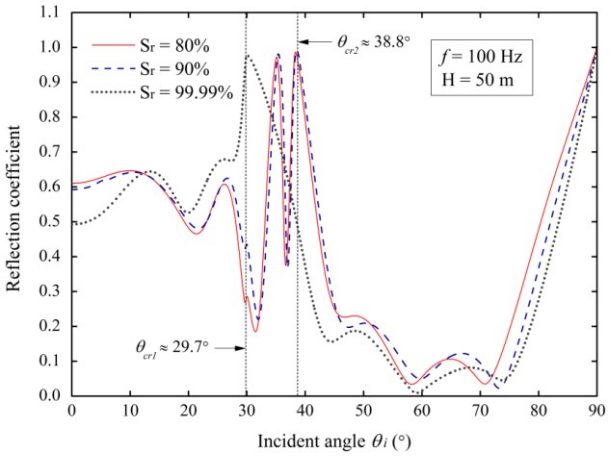

Figure 4. Reflection coefficient (A_r / A_i) as a function of incident angle θ_i for three different liquid saturations: Sr =80%, 90% and 99.99%.

4.3 Variation of reflection coefficient with the layer thickness

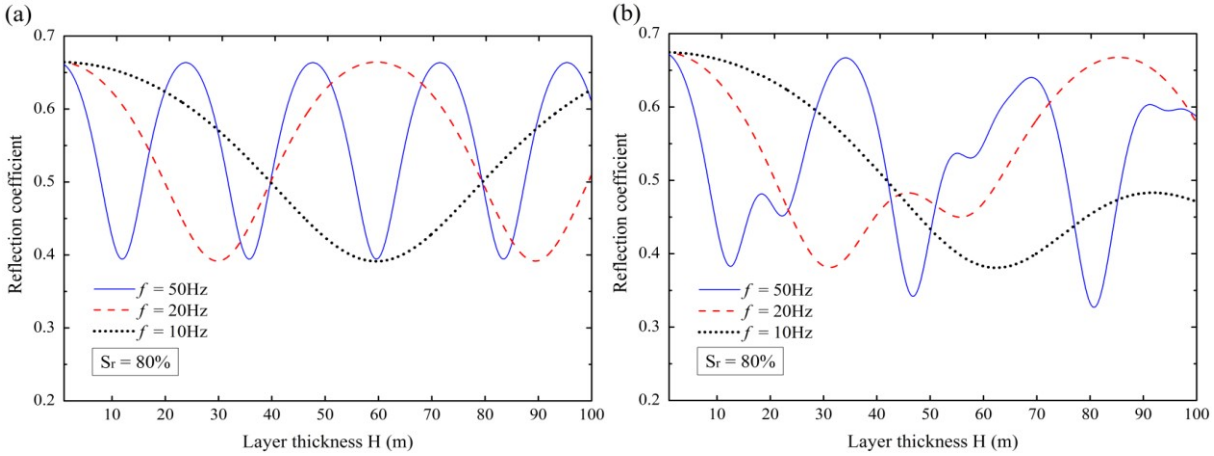

Figure 5. Reflection coefficient (A_r / A_i) as a function of layer thickness H for three different frequencies: f = 10Hz, 20Hz and 50Hz. (a) incident angle θ_i = 0° and (b) incident angle θ_i = 25°.

To analyze the effect of interlayer thickness on the reflection coefficient clearly, Figs. 5(a) and (b) show A_r / A_i in the overlying water as a function of layer thickness H (0m ≤ H ≤ 100m) at 10Hz, 20Hz and 50Hz, respectively. The liquid of the porous layer Sr is postulated to be 80%. In the case of θ_i = 0° (see Fig. 5(a)), the reflection coefficient fluctuates periodically with layer thickness. The oscillation of reflection coefficient results from the resonant response of the P waves in the porous layer. This is because when the incident wave strikes at the interface (z = 0) vertically from the overlying water, only three types of P waves (i.e., P1wave P2 wave and P3 wave) are generated in the lower gassy porous layer. Moreover, due to the high damping of the P2 and P3 waves, the P1wave could be viewed as the major factor affecting the reflection coefficient. In this low frequency range, the phase speed of P1 wave in porous layer is found to be frequency-independent and equals to 2384m/s. Therefore, the wavelengths of the P1 wave corresponding to 20Hz and 50Hz are nearly 119m and 48m, respectively. Meanwhile, it is shown in Fig. 5(a) that, the change circle of reflection coefficient in 20Hz and 50Hz approximate to 60m and 24m, respectively. This indicates that, at the normal incidence (i.e., θ_i = 0°), the change circle of reflection coefficient with respect to the thickness of the gassy poroelastic layer is equal to half of the wavelength of the P1 wave. However, when the incident wave is no longer perpendicular to the interface, there is a transmitted S wave other than the three types of transmitted P wave exist in the lower gassy porous layer. In this case, the reflection of the waves at the interface is simultaneously influenced by both P wave and S wave in the subjacent porous layer and hence the reflection coefficient becomes more indeterminate. For instance, when incident angle θ_i = 25° as demonstrated in Fig. 5(b), the reflection coefficient fluctuates with the increase of thickness irregularly. The effect of frequency on the reflection coefficient can also be revealed from both Figs. 5(a) and 5(b). The wave reflection upon the interface has a close correlation with wavelengths of the waves in the lower layer. With the increasing of frequency (i.e., decreasing of wavelength), the fluctuation of the reflection coefficient with layer thickness becomes more frequent.

4.4 Variation of reflection coefficient with the liquid saturation of the layer

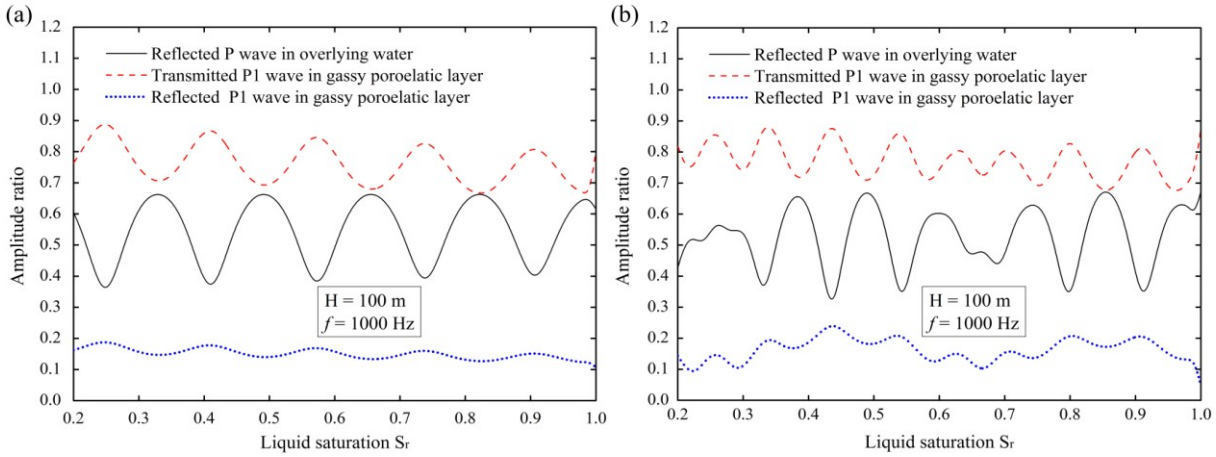

Figure 6. Amplitude ratios of the reflected wave (A_r / A_i), transmitted P1 wave (A_{tp1}^S / A_i) and reflected P1 wave (A_{rp1}^S / A_i) as a function of liquid saturation Sr. (a) incident angle $\theta_i = 0°$ and (b) incident angle $\theta_i = 25°$.

Figs. 6 (a) and (b) show the effect of the liquid saturation of the intermediate gassy porous layer on the amplitude ratios of the reflected P wave (i.e., reflection coefficient), transmitted P1 wave and reflected P1 wave, respectively. The liquid saturation degree Sr ranges from 20% to 99.99%. The thickness H is assumed to be 100m and the wave frequency f is taken to be 1000Hz. Similarly, the numerical results of the incident angle θ_i = 0° and 25° are given in Figs. 6 (a) and (b), respectively. When the incident wave spreads at the interface perpendicularly, all the amplitude ratios of the reflected P wave, transmitted P1 wave and reflected P1 wave almost fluctuate with liquid saturation periodically. While in the case of θ_i = 25°, the phenomenon of the fluctuation is observed to be relatively irregular.

Furthermore, it is worth noting that, in both of these two cases of different incident angles, the trend of reflected P wave in the upper water almost bear the opposite trend comparing with those of transmitted and reflected P1 waves in the lower porous layer. This phenomenon is due the energy conservation among the incident wave, reflected waves and transmitted waves.

Figs. 7(a) and (b) show the reflection coefficient as a function of liquid saturation at $\theta_i = 0°$ and 25°, respectively. The numerical results considering four different frequencies, i.e., f = 1Hz, 10Hz, 100Hz and 1000Hz, are presented. The layer thickness is 100m. As the same shown in Figs. 5(a) and (b), the influence of wave frequency on the reflection coefficient is remarkable. When the frequency is in low range, e.g., f = 1Hz, the effect of saturation change on the reflection coefficient is insignificant and the relationship between the reflection coefficient and change of saturation is almost linearly dependent. In other words, when the wavelength of the waves in lower layer is long enough, the effect of saturation change could be negligible. With the increasing of frequency, the fluctuation of the reflection coefficient with liquid saturation becomes more notable. It is also noteworthy that, in Fig. 7(b), when the saturation approaches fully saturated state, the calculation results for different frequencies tend to converge at $A_r / A_i \approx 0.67$.

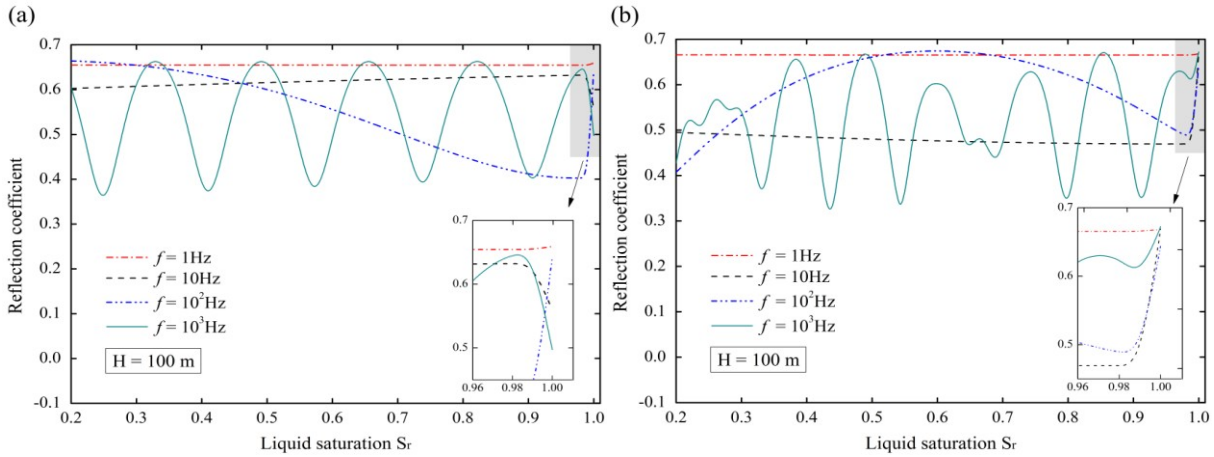

Figure 7. Reflection coefficient (A_r / A_i) as a function of liquid saturation Sr for four different frequencies: f = 1Hz, 10Hz, 100Hz and 1000Hz. (a) incident angle θ_i = 0° and (b) incident angle θ_i = 25°.

5 CONCLUSIONS

- In the sandwiched gassy poroelastic layer, one transverse wave and three longitudinal waves coexist at oblique incidence. In these various mode waves, P1 and S wave propagate faster and attenuate relatively slowly, and thus influence the wave reflection characteristics at the surface of the porous layer significantly.
- The numerical results indicate that the incident angle renders a significant influence on the amplitude ratio of the reflected wave, i.e., reflection coefficient. It is also shown that, the reflection coefficient attains its maximum value at θi = θcr1 ~ θcr2, where θcr1 and θcr2 denote the critical incident angles for the two limiting cases (H = 0 and H ≈ ∞).
- When the incident wave strikes upon the interface perpendicularly, the reflection coefficient seems to fluctuate periodically with the layer thickness. However, if the plane wave is not normally incident, a transmitted S wave is generated, and the reflection coefficient fluctuates with the increase of the thickness irregularly. With the increasing of frequency, the fluctuation of the reflection coefficient with layer thickness becomes more frequent.
- It is found that, in the low frequency range, the effect of saturation change on the reflection coefficient is not obvious. With the increasing of frequency, the fluctuation of the reflection coefficient with liquid saturation becomes more significant.Papers must be translated to Portable Document Format (PDF) before submission through the Conference website.

Appendix:

The explicit expressions of the elements of $[M]$ are given as follows:

$$m_{1,1} = -K_W k_{rp}^{\ 2},\ m_{1,2} = (r_{SS} + n_S\lambda_S + r_{SL}\delta_{L1} + r_{SG}\delta_{G1} + 2n_S\mu_S n_{tp1}^{\ 2})k_{tp1}^{\ 2},$$

$$m_{1,3} = (r_{SS} + n_S\lambda_S + r_{SL}\delta_{L2} + r_{SG}\delta_{G2} + 2n_S\mu_S n_{tp2}^{\ 2})k_{tp2}^{\ 2},\ m_{1,4} = (r_{SS} + n_S\lambda_S + r_{SL}\delta_{L3} + r_{SG}\delta_{G3} + 2n_S\mu_S n_{tp3}^{\ 2})k_{tp3}^{\ 2},$$

$$m_{1,5} = (r_{SS} + n_S\lambda_S + r_{SL}\delta_{L1} + r_{SG}\delta_{G1} + 2n_S\mu_S n_{rp1}^{\ 2})k_{rp1}^{\ 2},\ m_{1,6} = (r_{SS} + n_S\lambda_S + r_{SL}\delta_{L2} + r_{SG}\delta_{G2} + 2n_S\mu_S n_{rp2}^{\ 2})k_{rp2}^{\ 2},$$

$$m_{1,7} = (r_{SS} + n_S\lambda_S + r_{SL}\delta_{L3} + r_{SG}\delta_{G3} + 2n_S\mu_S n_{rp3}^{\ 2})k_{rp3}^{\ 2},\ m_{1,8} = -2n_S\mu_S l_{ts} n_{ts} k_{ts}^{\ 2},\ m_{1,9} = 2n_S\mu_S l_{rs} n_{rs} k_{rs}^{\ 2},$$

$$m_{1,10} = 0,\ m_{1,11} = 0;\ m_{2,1} = -n_{rp}k_{rp},\ m_{2,2} = -n_{tp1}k_{tp1},\ m_{2,3} = -n_{tp2}k_{tp2},\ m_{2,4} = -n_{tp3}k_{tp3},\ m_{2,5} = n_{rp1}k_{rp1},$$

$$m_{2,6} = n_{rp2}k_{rp2},\ m_{2,7} = n_{rp3}k_{rp3},\ m_{2,8} = l_{ts}k_{ts},\ m_{2,9} = l_{rs}k_{rs},\ m_{2,10} = 0,\ m_{2,11} = 0;\ m_{3,1} = 0,$$

$$m_{3,2} = (\delta_{L1} - 1)n_{tp1}k_{tp1},\ m_{3,3} = (\delta_{L2} - 1)n_{tp2}k_{tp2},\ m_{3,4} = (\delta_{L3} - 1)n_{tp3}k_{tp3},\ m_{3,5} = (1 - \delta_{L1})n_{rp1}k_{rp1},$$

$m_{3,6}=(1-\delta_{L2})n_{rp2}k_{rp2}$, $m_{3,7}=(1-\delta_{L3})n_{rp3}k_{rp3}$, $m_{3,8}=l_{ts}k_{ts}(1-\delta_{LS})$, $m_{3,9}=l_{rs}k_{rs}(1-\delta_{LS})$, $m_{3,10}=0$,
$m_{3,11}=0$; $m_{4,1}=0$, $m_{4,2}=(\delta_{G1}-1)n_{tp1}k_{tp1}$, $m_{4,3}=(\delta_{G2}-1)n_{tp2}k_{tp2}$, $m_{4,4}=(\delta_{G3}-1)n_{tp3}k_{tp3}$,
$m_{4,5}=(1-\delta_{G1})n_{rp1}k_{rp1}$, $m_{4,6}=(1-\delta_{G2})n_{rp2}k_{rp2}$, $m_{4,7}=(1-\delta_{G3})n_{rp3}k_{rp3}$, $m_{4,8}=l_{ts}k_{ts}(1-\delta_{GS})$,
$m_{4,9}=l_{rs}k_{rs}(1-\delta_{GS})$, $m_{4,10}=0$, $m_{4,11}=0$; $m_{5,1}=0$, $m_{5,2}=2n_{tp1}l_{tp1}k_{tp1}^{\ 2}$, $m_{5,3}=2n_{tp2}l_{tp2}k_{tp2}^{\ 2}$,
$m_{5,4}=2n_{tp3}l_{tp3}k_{tp3}^{\ 2}$, $m_{5,5}=-2n_{rp1}l_{rp1}k_{rp1}^{\ 2}$, $m_{5,6}=-2n_{rp2}l_{rp2}k_{rp2}^{\ 2}$, $m_{5,7}=-2n_{rp3}l_{rp3}k_{rp3}^{\ 2}$, $m_{5,8}=(n_{ts}^{\ 2}-l_{ts}^{\ 2})k_{ts}^{\ 2}$,
$m_{5,9}=(n_{rs}^{\ 2}-l_{rs}^{\ 2})k_{rs}^{\ 2}$, $m_{5,10}=0$, $m_{5,11}=0$; $m_{6,1}=0$, $m_{6,2}=-n_{tp1}k_{tp1}\exp(\mathrm{i}n_{tp1}k_{tp1}\mathrm{H})$,
$m_{6,3}=-n_{tp2}k_{tp2}\exp(\mathrm{i}n_{tp2}k_{tp2}\mathrm{H})$, $m_{6,4}=-n_{tp3}k_{tp3}\exp(\mathrm{i}n_{tp3}k_{tp3}\mathrm{H})$, $m_{6,5}=n_{rp1}k_{rp1}\exp(-\mathrm{i}n_{rp1}k_{rp1}\mathrm{H})$,
$m_{6,6}=n_{rp2}k_{rp2}\exp(-\mathrm{i}n_{rp2}k_{rp2}\mathrm{H})$, $m_{6,7}=n_{rp3}k_{rp3}\exp(-\mathrm{i}n_{rp3}k_{rp3}\mathrm{H})$, $m_{6,8}=l_{ts}k_{ts}\exp(\mathrm{i}n_{ts}k_{ts}\mathrm{H})$,
$m_{6,9}=l_{rs}k_{rs}\exp(-\mathrm{i}n_{rs}k_{rs}\mathrm{H})$, $m_{6,10}=n_{pe}k_{pe}\exp(\mathrm{i}n_{pe}k_{pe}\mathrm{H})$, $m_{6,11}=-l_{se}k_{se}\exp(\mathrm{i}n_{se}k_{se}\mathrm{H})$; $m_{7,1}=0$,
$m_{7,2}=l_{tp1}k_{tp1}\exp(\mathrm{i}n_{tp1}k_{tp1}\mathrm{H})$, $m_{7,3}=l_{tp2}k_{tp2}\exp(\mathrm{i}n_{tp2}k_{tp2}\mathrm{H})$, $m_{7,4}=l_{tp3}k_{tp3}\exp(\mathrm{i}n_{tp3}k_{tp3}\mathrm{H})$,
$m_{7,5}=l_{rp1}k_{rp1}\exp(-\mathrm{i}n_{rp1}k_{rp1}\mathrm{H})$, $m_{7,6}=l_{rp2}k_{rp2}\exp(-\mathrm{i}n_{rp2}k_{rp2}\mathrm{H})$, $m_{7,7}=l_{rp3}k_{rp3}\exp(-\mathrm{i}n_{rp3}k_{rp3}\mathrm{H})$,
$m_{7,8}=n_{ts}k_{ts}\exp(\mathrm{i}n_{ts}k_{ts}\mathrm{H})$, $m_{7,9}=-n_{rs}k_{rs}\exp(-\mathrm{i}n_{rs}k_{rs}\mathrm{H})$, $m_{7,10}=-l_{pe}k_{pe}\exp(\mathrm{i}n_{pe}k_{pe}\mathrm{H})$,
$m_{7,11}=-n_{se}k_{se}\exp(\mathrm{i}n_{se}k_{se}\mathrm{H})$;

$m_{8,1}=0$, $m_{8,2}=-2n_S\mu_S n_{tp1}l_{tp1}k_{tp1}^{\ 2}\exp(\mathrm{i}n_{tp1}k_{tp1}\mathrm{H})$, $m_{8,3}=-2n_S\mu_S n_{tp2}l_{tp2}k_{tp2}^{\ 2}\exp(\mathrm{i}n_{tp2}k_{tp2}\mathrm{H})$,
$m_{8,4}=-2n_S\mu_S n_{tp3}l_{tp3}k_{tp3}^{\ 2}\exp(\mathrm{i}n_{tp3}k_{tp3}\mathrm{H})$, $m_{8,5}=2n_S\mu_S n_{rp1}l_{rp1}k_{rp1}^{\ 2}\exp(-\mathrm{i}n_{rp1}k_{rp1}\mathrm{H})$,
$m_{8,6}=2n_S\mu_S n_{rp2}l_{rp2}k_{rp2}^{\ 2}\exp(-\mathrm{i}n_{rp2}k_{rp2}\mathrm{H})$, $m_{8,7}=2n_S\mu_S n_{rp3}l_{rp3}k_{rp3}^{\ 2}\exp(-\mathrm{i}n_{rp3}k_{rp3}\mathrm{H})$,
$m_{8,8}=(l_{ts}^{\ 2}-n_{ts}^{\ 2})n_S\mu_S k_{ts}^{\ 2}\exp(\mathrm{i}n_{ts}k_{ts}\mathrm{H})$, $m_{8,9}=(l_{rs}^{\ 2}-n_{rs}^{\ 2})n_S\mu_S k_{rs}^{\ 2}\exp(-\mathrm{i}n_{rs}k_{rs}\mathrm{H})$,
$m_{8,10}=2\mu_E n_{pe}l_{pe}k_{pe}^{\ 2}\exp(\mathrm{i}n_{pe}k_{pe}\mathrm{H})$, $m_{8,11}=(n_{se}^{\ 2}-l_{se}^{\ 2})\mu_E k_{se}^{\ 2}\exp(\mathrm{i}n_{se}k_{se}\mathrm{H})$; $m_{9,1}=0$,
$m_{9,2}=-(r_{SS}+n_S\lambda_S+r_{SL}\delta_{L1}+r_{SG}\delta_{G1}+2n_S\mu_S n_{tp1}^{\ 2})k_{tp1}^{\ 2}\exp(\mathrm{i}n_{tp1}k_{tp1}\mathrm{H})$,
$m_{9,3}=-(r_{SS}+n_S\lambda_S+r_{SL}\delta_{L2}+r_{SG}\delta_{G2}+2n_S\mu_S n_{tp2}^{\ 2})k_{tp2}^{\ 2}\exp(\mathrm{i}n_{tp2}k_{tp2}\mathrm{H})$,

$m_{9,4}=-(r_{SS}+n_S\lambda_S+r_{SL}\delta_{L3}+r_{SG}\delta_{G3}+2n_S\mu_S n_{tp3}^{\ 2})k_{tp3}^{\ 2}\exp(\mathrm{i}n_{tp3}k_{tp3}\mathrm{H})$,

$m_{9,5}=-(r_{SS}+n_S\lambda_S+r_{SL}\delta_{L1}+r_{SG}\delta_{G1}+2n_S\mu_S n_{rp1}^{\ 2})k_{rp1}^{\ 2}\exp(-\mathrm{i}n_{rp1}k_{rp1}\mathrm{H})$,
$m_{9,6}=-(r_{SS}+n_S\lambda_S+r_{SL}\delta_{L2}+r_{SG}\delta_{G2}+2n_S\mu_S n_{rp2}^{\ 2})k_{rp2}^{\ 2}\exp(-\mathrm{i}n_{rp2}k_{rp2}\mathrm{H})$,
$m_{9,7}=-(r_{SS}+n_S\lambda_S+r_{SL}\delta_{L3}+r_{SG}\delta_{G3}+2n_S\mu_S n_{rp3}^{\ 2})k_{rp3}^{\ 2}\exp(-\mathrm{i}n_{rp3}k_{rp3}\mathrm{H})$, $m_{9,8}=2n_S\mu_S l_{ts}n_{ts}k_{ts}^{\ 2}\exp(\mathrm{i}n_{ts}k_{ts}\mathrm{H})$,
$m_{9,9}=-2n_S\mu_S l_{rs}n_{rs}k_{rs}^{\ 2}\exp(-\mathrm{i}n_{rs}k_{rs}\mathrm{H})$, $m_{9,10}=(\lambda_E+2\mu_E n_{pe}^{\ 2})k_{pe}^{\ 2}\exp(\mathrm{i}n_{pe}k_{pe}\mathrm{H})$,
$m_{9,11}=-2\mu_E n_{se}l_{se}k_{se}^{\ 2}\exp(\mathrm{i}n_{se}k_{se}\mathrm{H})$; $m_{10,1}=0$, $m_{10,2}=(\delta_{L1}-1)n_{tp1}k_{tp1}\exp(\mathrm{i}n_{tp1}k_{tp1}\mathrm{H})$,
$m_{10,3}=(\delta_{L2}-1)n_{tp2}k_{tp2}\exp(\mathrm{i}n_{tp2}k_{tp2}\mathrm{H})$, $m_{10,4}=(\delta_{L3}-1)n_{tp3}k_{tp3}\exp(\mathrm{i}n_{tp3}k_{tp3}\mathrm{H})$,
$m_{10,.5}=(1-\delta_{L1})n_{rp1}k_{rp1}\exp(-\mathrm{i}n_{rp1}k_{rp1}\mathrm{H})$, $m_{10,6}=(1-\delta_{L2})n_{rp2}k_{rp2}\exp(-\mathrm{i}n_{rp2}k_{rp2}\mathrm{H})$,
$m_{10,7}=(1-\delta_{L3})n_{rp3}k_{rp3}\exp(-\mathrm{i}n_{rp3}k_{rp3}\mathrm{H})$, $m_{10,8}=l_{ts}k_{ts}(1-\delta_{LS})\exp(\mathrm{i}n_{ts}k_{ts}\mathrm{H})$,
$m_{10,9}=l_{rs}k_{rs}(1-\delta_{LS})\exp(-\mathrm{i}n_{rs}k_{rs}\mathrm{H})$, $m_{10,10}=0$, $m_{10,11}=0$; $m_{11,1}=0$, $m_{11,2}=(\delta_{G1}-1)n_{tp1}k_{tp1}\exp(\mathrm{i}n_{tp1}k_{tp1}\mathrm{H})$,
$m_{11,3}=(\delta_{L2}-1)n_{tp2}k_{tp2}\exp(\mathrm{i}n_{tp2}k_{tp2}\mathrm{H})$, $m_{11,4}=(\delta_{L3}-1)n_{tp3}k_{tp3}\exp(\mathrm{i}n_{tp3}k_{tp3}\mathrm{H})$,
$m_{11,5}=(1-\delta_{G1})n_{rp1}k_{rp1}\exp(-\mathrm{i}n_{rp1}k_{rp1}\mathrm{H})$, $m_{11,6}=(1-\delta_{G2})n_{rp2}k_{rp2}\exp(-\mathrm{i}n_{rp2}k_{rp2}\mathrm{H})$,
$m_{11,7}=(1-\delta_{G3})n_{rp3}k_{rp3}\exp(-\mathrm{i}n_{rp3}k_{rp3}\mathrm{H})$, $m_{11,8}=l_{ts}k_{ts}(1-\delta_{GS})\exp(\mathrm{i}n_{ts}k_{ts}\mathrm{H})$,
$m_{11,9}=l_{rs}k_{rs}(1-\delta_{GS})\exp(-\mathrm{i}n_{rs}k_{rs}\mathrm{H})$, $m_{11,10}=0$, $m_{11,11}=0$;

The explicit expressions of the elements of $[Q]$ are as follows:

$q_1 = K_W k_{ip}^2$, $q_2 = -n_{ip} k_{ip}$, $q_3 = 0$, $q_4 = 0$, $q_5 = 0$, $q_6 = 0$, $q_7 = 0$, $q_8 = 0$, $q_9 = 0$, $q_{10} = 0$, $q_{10} = 0$, $q_{11} = 0$.

REFERENCES

[1] J. Geertsma, D.C. Smit, Some aspects of elastic wave propagation in fluid-saturated porous solids, *Geophysics,* **26**, 169–181, 1961.

[2] R.D. Stoll, T.K. Kan, Reflection of acoustic wave at a water-sediment interface, *J. acoust. Soc. Am.*, **70**, 149–156, 1981.

[3] K. Wu, Q. Xue, L. Adler, Reflection and transmission of elastic waves from a fluid saturated porous solid boundary, *J. acoust. Soc. Am.*, **87**, 2349–2358, 1990.

[4] J.E. Santos, J.M. Corbero, C.L. Ravazzoli, J.L. Hensley, Reflection transmission coefficients in fluid–saturated porous media, *J. acoust. Soc. Am.*, **91**, 1911–1923, 1992.

[5] A. Madeo, S. Gavrilyuk, Propagation of acoustic waves in porous media and their reflection and transmission at a pure-fluid/porous-medium permeable interface, *Eur. J. Mech. A-Solid.*, **29**, 897–910, 2010.

[6] M.D. Sharma, M. Kumar, Reflection of attenuated wave s at the surface of a porous solid saturated with two immiscible viscous fluids, *Geophys. J. I nt.* **184**, 371–384, 2011.

[7] M.A. Biot, Theory of propagation of elastic waves in a fluid-saturated porous solid. I. Low-frequency range, *J. acoust. Soc. Am.*, **28**,168–178, 1956.

[8] T.J. Plona, Observation of a second bulk compressional wave in a porous medium at ultrasonic frequencies, *Appl. Phys. Lett.* 36, 259–261, 1980.

[9] P. Nagy, L. Adler, B. Bonner, Slow wave propagation in air-filled porous materials and natural rocks, *Appl. Phys. Lett.* **56**, 2504–2506, 1990.

[10] K.L. Williams, An effective fluid model for acoustic propagation in sediments derived from Biot theory, *J. acoust. Soc. Am.*, **110**, 2276–2281, 2001.

[11] N.P. Chotiros, M.J. Isakson, A broadband model of sandy ocean sediments: Biot-Stoll with contact squirt flow and shear drag, *J. acoust. Soc. Am.*, **116**, 2011-2022, 2004.

[12] K. Ohkawa, Confirmation of the Biot theory for water-saturated sands at high frequencies and effects of scattering on the attenuation of sound waves, *J. acoust. Soc. Am.*, **119**, 709–711, 2006.

[13] D.G. Albert, A comparison between wave propagation in water-saturated and air-saturated porous materials, *Appl. Phys. Lett.*, **73**, 28–36, 1993.

[14] A.I.M. Denneman, G.G. Drijkoningen, D.M.J. Smeulders, K. Wapenaar, Reflection and transmission of waves at a fluid/porous-medium interface, *Geophysics,* **67**, 282–291, 2002.

[15] B.H. Russell, K. Hedlin, F.J. Hilterman, L. R. Lines, Fluid-property discrimination with AVO: A Biot-Gassmann perspective, *Geophysics*, 68, 29-39, 2003.

[16] K. Ohkawa, H. Yamaoka, T. Yamamoto, Acoustic backscattering from a sandy seabed, *IEEE. J. Oceanic. Eng.,* **30**, 700–708, 2005.

[17] Z.J. Dai, Z.B. Kuang, Reflection and transmission of elastic waves at the interface between water and a double porosity solid, *Transport. Porous. Med.*, **72**, 369–392, 2008.

[18] E.Y.T. Kuo, Acoustic wave scattering from two solid boundaries at the ocean bottom: Reflection loss, *IEEE. J. Oceanic. Eng.,* **17**, 159–170, 1992.

[19] M.A. Ainslie, Reflection transmission coefficients for a layered fluid sediment overlying a uniform solid substrate, *J. acoust. Soc. Am.*, **99**, 893–902, 1996.

[20] J.T. Wang, F. Jin, C.H. Zhang, Reflection and transmission of plane waves at an interface of water/porous sediment with underlying solid substrate, *Ocean. Eng.,* **63**, 8–16, 2013.

[21] D.D. Lyu, J.T. Wang, F. Jin, C.H. Zhang, Reflection and transmission of plane waves at a water–porous sediment interface with a double porosity substrate, *Transport. Porous. Med.,* **103**, 25–45, 2014.

[22] F.A. Boyle, N.P. Chotiros, A model for high frequency backscatter from gas bubbles in sandy sediments, *J. acoust. Soc. Am.*, **98**, 531–541, 1995.

[23] C. Wei, K.K. Muraleetharan, A continuum theory of porous media saturated by multiple immiscible fluids: I. Linear poroelasticity, *Int. J.Eng. Sci.*, **40**, 1807–1833, 2002.

[24] W.C. Lo, E. Majer, G. Sposito, Wave propagation through elastic porous media containing two immiscible fluids, *Water. Resour. Res.,* **41**, 1–20, 2005.

[25] J.F. Lu, A. Hanyga, Linear dynamic model for porous media saturated by two immiscible fluids, *Int. J. Solids. Struct.,* **42**, 2689–2709, 2005.

[26] B. Albers, Analysis of the propagation of sound waves in partially saturated soils by means of a macroscopic linear poroelastic model, *Transport. Porous. Med.,***80**, 173–192, 2009.

[27] W.Y. Chen, T.D. Xia, W.T. Hu, A mixture theory analysis for the surface-wave propagation in an unsaturated porous medium, *Int. J. Solids. Struct.,* **48**, 2402–2412, 2011.

[28] C.L. Yeh, W.C. Lo, C.D. Jan, C.C. Yang, Reflection and refraction of obliquely incident elastic waves upon the interface between two porous elastic half-spaces saturated by different fluid mixtures, *J Hydrol.* **395**, 91–102, 2010.

[29] W.Y. Chen, T.D. Xia, M.M. Sun, C.J. Zhai, Transverse wave at a plane interface between isotropic elastic and unsaturated porous elastic solid half-spaces, *Transport. Porous. Med.,***94**, 417–436, 2012.

[30] K.K. Muraleetharan, C. Wei, Dynamic behaviour of unsaturated porous media: Governing equations using the theory of mixtures with interfaces (TMI). *Int. J. Numer. Anal. Methods. Geomech.* **23**, 1579–1608, 1999.

[31] S.K. Garg, A.H. Nayfeh, Compressional wave propagation in liquid and or gas saturated elastic porous media. *J. Appl. Phys.*, **60**, 3045–3055, 1986.

[32] J.G. Berryman, L. Thigpen, R.C.Y. Chin, Bulk elastic wave propagation in partially saturated porous solids, *J. acoust. Soc. Am.*, **84**, 360–373, 1988.

[33] J. Fatti, G. Smith, P. Vail, P. Strauss, P. Levitt, Detection of gas in sandstone reservoirs using AVO analysis: a 3D Seismic Case History Using the Geostack Technique, *Geophysics*, **59**, 1362-1376, 1994.

[34] Russell, B.H., Hedlin, K., Hilterman, F.J. Lines, L. R., 2003. Fluid-property discrimination with AVO: A Biot-Gassmann perspective, *Geophysics*, **68**, 29-39.

[35] W.C. Lo, G. Sposito, E. Majer, Low-frequency dilatational wave propagation through unsaturated porous media containing two immiscible fluids. *Transp*. *Porous*. *Med.*, **68**, 91–105, 2007.